Materials Today Bio 2 (2019) 100005

Contents lists available at ScienceDirect

Materials Today Bio

journal homepage: www.journals.elsevier.com/materials-today-bio

Biomimetic hydroxyapatite/collagen composite drives bone niche recapitulation in a rabbit orthotopic model

S. Minardi [a,b,e,1], F. Taraballi [a,d], F.J. Cabrera [a], J. Van Eps [a], X. Wang [a], S.A. Gazze [c], Joseph S. Fernandez-Mourev [e,f], A. Tampieri [b], L. Francis [c], B.K. Weiner [a,d], E. Tasciotti [a,d,e,*]

[a] Center for Musculoskeletal Regeneration, Houston Methodist Research Institute (HMRI), 6670 Bertner Ave. Houston, TX 77030, USA
[b] National Research Council of Italy, Institute of Science and Technology for Ceramics (ISTEC-CNR), Via Granarolo 64, 48018 Faenza, RA Italy
[c] Reproductive Biology and Gynaecological Oncology Group, Swansea University Medical School, Singleton Park, Swansea SA2 8PP, UK
[d] Houston Methodist Orthopedic and Sports Medicine, 6565 Fannin Street, Houston, TX 77030, USA
[e] Center for Biomimetic Medicine, Houston Methodist Research Institute (HMRI), 6670 Bertner Ave. Houston, TX 77030, USA
[f] Department of Surgery, Houston Methodist Hospital, 6565 Fannin St., Suite 1660, Houston, TX 77030, USA

ARTICLE INFO

Keywords:
Bone regeneration
Hydroxyapatite
Collagen
Biomimetic material
Stem cell

ABSTRACT

Synthetic osteoinductive materials that mimic the human osteogenic niche have emerged as ideal candidates to address this area of unmet clinical need. In this study, we evaluated the osteoinductive potential in a rabbit orthotopic model of a magnesium-doped hydroxyapatite/type I collagen (MHA/Coll) composite. The composite was fabricated to exhibit a highly fibrous structure of carbonated MHA with 70% (±2.1) porosity and a Ca/P ratio of 1.5 (±0.03) as well as a diverse range of elasticity separated to two distinct stiffness peaks of low (2.35 ± 1.16 MPa) and higher (9.52 ± 2.10 MPa) Young's Modulus. Data suggested that these specific compositional and nanomechanical material properties induced the deposition of *de novo* mineral phase, while modulating the expression of early and late osteogenic marker genes, in a 3D *in vitro* model using human bone marrow-derived mesenchymal stem cells (hBM-MSCs). When tested in the rabbit orthotopic model, MHA/Col1 scaffold induction of new trabecular bone mass was observed by DynaCT scan, only 2 weeks after implantation. Bone histomorphometry at 6 weeks revealed a significant amount of *de novo* bone matrix formation. qPCR demonstrated MHA/Coll scaffold full cellularization *in vivo* and the expression of both osteogenesis-associated genes (*Spp1, Sparc, Col1a1, Runx2, Dlx5*) as well as hematopoietic (*Vcam1, Cd38, Sele, Kdr*) and bone marrow stromal cell marker genes (*Vim, Itgb1, Alcam*). Altogether, these data provide evidence of the solid osteoinductive potential of MHA/Coll and its suitability for multiple approaches of bone regeneration.

1. Introduction

A variety of medical conditions (e.g. traumas, diseases, deformities, tumor resection) may require bone augmentation and reconstruction strategies [1]. Autograft (i.e. patient's iliac crest-derived bone), allograft (i.e. cadaveric bone), and demineralized allograft (or demineralized bone matrix, DBM) are the most common bone-graft substitutes used in orthopedic surgery [2–5]. These types of grafts have limitations such as pain (i.e. autograft), limited supply, or a potential allogenic response (i.e. allograft) [6]. Administration of exogenous growth factors eliciting the differentiation of progenitor cells to enhance bone regeneration has emerged as a valid alternative approach [7]. Since its FDA approval in 2002, the use of recombinant human bone morphogenetic protein-2 adsorbed on a collagen sponge (INFUSE™) has been used as a bone graft substitute to improve clinical outcomes [8–10]. However, severe side-effects were linked to the superphysiological dosing of the growth factor [11], and its use in clinical practice remains highly controversial [12,13]. Stem cell–mediated bone repair has also been tested in various clinical settings of bone reconstruction [14]. However, the higher level of complexity and cost associated with cell-based bone regeneration therapies have limited its widespread use in orthopedic surgery [15].

Many research groups have focused on developing controlled delivery systems to decrease BMP-2 doses and limit its side-effects or to deliver patient's cells more efficiently, however, engineering an osteogenic

* Corresponding author.Houston Methodist Research Institute (HMRI) 6670 Bertner Ave. Houston, TX 77030, USA.
E-mail address: etasciotti@houstonmethodist.org (E. Tasciotti).
[1] Present Address: Department of Orthopaedic Surgery, Northwestern University Feinberg School of Medicine; Simpson Querrey Institute for BioNanotechnology, Northwestern University, 303 E. Superior Street, Chicago, IL 60611.

https://doi.org/10.1016/j.mtbio.2019.100005
Received 21 December 2018; Received in revised form 2 April 2019; Accepted 14 April 2019
Available online 20 April 2019

growth factor–free and cell-free synthetic scaffold for bone regeneration remains highly desirable [16,17].

Growth factor–free and cell-free composite scaffolds fabricated from hydroxyapatite, tricalcium phosphate ceramics, and polymer binders (e.g. PLA, PLGA) have been proposed with mixed outcomes [5,18–21]. None of the current scaffolds have been applied clinically with fully satisfactory performance and safety, compared with Infuse™ [22].

Among composite materials for bone regeneration, biohybrid composite fabricated through bioinspired mineralization processes revealed to be highly successful in a few pioneer clinical studies in Europe [23–26]. During the synthesis of such composites—just like in the bone—an organic template (i.e. collagen type I) drives the nucleation of the mineral phase (i.e. hydroxyapatite), which is directly deposited within the organic matrix [27], resulting in a composite material that more closely resembles bone [28]. These biohybrid composites proved highly successful in a few pioneer clinical studies of posterolateral spinal fusion and osteochondral repair [23–26,29,30].

Toward this end, we recently optimized a biohybrid composite scaffold consisting of magnesium-doped hydroxyapatite/type I collagen (MHA/Coll), synthesized through a biologically inspired approach, which recapitulates bone biomineralization [28]. In the present study, we aimed at evaluating the osteoconductive potential of MHA/Coll in a rabbit orthotopic model of non–load-bearing bone augmentation. Although we previously demonstrated the osteogenic potential of this material in a subcutaneous ectopic site [28], in the present study, we investigated whether MHA/Coll could also induce bone formation in a larger orthotopic model, without any heterologous growth factors or cells. A biomimetic 3D *in vitro* cell culture system was used to investigate the osteogenic differentiation of human bone marrow–derived mesenchymal stem cells (hBM-MSCs) induced by MHA/Coll. Its ability to sequentially orchestrate the expression of crucial ostegenesis-associated genes and overall harmonize the *in vitro* osteogenic differentiation of hBM-MSCs was assessed by qPCR. *In vivo*, we investigated the ability of MHA/Coll to fully recapitulate a regenerative bone niche, to not only induce bone formation but also by assessing the presence of cells expressing hematopoiesis-associated marker genes within the core of the scaffold, like in mature bone.

2. Materials and methods

2.1. Fabrication of MHA/Coll

The scaffold was synthesized as previously described [28]. Briefly, bovine type I collagen (Nitta Casings Inc.) was dissolved at a concentration of 10 mg/mL in acetate buffer at pH 3.5. H_3PO_4 was added to 100 g of the acetic collagen dough (40 mM), homogenized with a mechanical blender, and then dropped in a solution of $Ca(OH)_2$ (40 mM) and $MgCl_2{\cdot}6H_2O$ (2 mM) in deionized (DI) water. The material underwent a wet crosslinking in an aqueous solution of 1,4-butanediol diglycidyl ether (2.5 mM), at 4 °C. After crosslinking, MHA/Coll was washed three times with DI water. The resulting slurry was molded in 48-well plates at a thickness of 2 mm, to fabricate the scaffold for the *in vitro* studies, whereas, for the *in vivo* studies, a cylindrical mold (4 cm × 1 cm) was used. The final interconnected porosity of the scaffold was generated by freeze drying. Briefly, the materials were frozen from +20 °C to −20 °C in 3 h and then heated from −20 °C to +20 °C in 5 h under vacuum conditions (20 mTorr). Non-mineralized collagen scaffolds (Coll) were also synthesized as previously described [28], as controls. All chemicals were purchased from Sigma Aldrich.

2.2. Characterization of MHA/Coll through scanning electron microscopy-energy-dispersive X-ray spectroscopy (EDS)

The morphology of MHA/Coll was assessed by a FEI Quanta 400 scanning electron microscopy (SEM), coupled with an energy-dispersive X-ray spectroscopy (EDX) detector (analyzing program: EDAX Genesis) (n = 3).

Scaffolds were sputter coated with 10 nm of Pt/Pd, via a Plasma Sciences CrC-150 Sputtering System (Torr International, Inc), and imaged at a voltage of 10 kV.

2.3. Fourier-transformed infrared spectroscopy

Fourier-transformed infrared spectroscopy (FTIR) was performed using a Nicolet 4700 Spectrometer (n = 3). KBr pellets of 10 mm in diameter were prepared by mixing 2 mg of grounded sample with 100 mg of KBr. Sixty-four runs were performed per sample. Spectra were analyzed by the software EZ OMNIC (Nicolet) after baseline correction.

2.4. Thermal gravimetric analysis

The amount of mineral phase nucleated on the organic template (type I collagen) was quantified by thermal gravimetric analysis (TGA). The samples (n = 3) were placed in alumina pans and subjected to a heating ramp from 25 °C to 800 °C, at 10 °C/min. A Q-600 TGA was used (TA Instruments).

2.5. Scaffold porosity

The volumes of the scaffolds (cylinders of 6 mm cm x 6 cm) (V_s) were calculated from their geometry. The porosity of the scaffolds was calculated as described elsewhere, through an ethanol adsorption method [31]. Values are expressed as means ± standard deviation (n = 3).

2.6. Nanomechanical testing

The elastic properties of MHA/Coll were evaluated with atomic force microscopy (AFM) by extracting the Young's modulus from AFM-acquired force curves; a BioScope Catalyst AFM (Bruker Instruments) was used, in tandem with MLCT-E silicon nitride cantilevers, with spring constant and deflection sensitivity experimentally determined before each measurement. For each scaffold (n = 3), 18 different 4-μm^2 areas were considered, with 100 equally spaced force curves obtained on each area. The contact regime of the approach part of each force curve was fitted with the equation of a spherical indenter (Hertz model, Eq. (1)), using the fitting module of Nanoscope Analysis software, v1.50, and the elastic module (Young's module) in each force curve was extracted according to Eq. (1):

$$F = \frac{4E\sqrt{R}\delta^{3/2}}{3(1-\upsilon^2)} \quad (1)$$

In Eq. (1), F is the force applied by the cantilever tip to the scaffold (5 nN), E is the Young's modulus (fit parameter), υ is the Poissons ratio (0.5), and R the radius of the indenter of the cantilever tip (20 nm). Only force curves with a goodness of fit to Eq. (1) between 0.85 and 1 were considered. Data distribution and statistical analysis were performed using Wolfram Mathematica 9.0 and Minitab, v.14.1.

2.7. 3D culture of hBM-MSC on MHA/Coll

The hBM-MSCs used in the present study were isolated from the bone marrow of two women (aged 28 and 35, respectively), at the Texas A&M Institute for Regenerative Medicine (Temple, TX, USA). 10^4 cells/cm^2 were seeded and incubated at 37 °C in humidified atmosphere (90%) with 5% CO_2 and 5% O_2.

The medium utilized was composed of α-minimum essential media (MEM), 10% fetal bovine serum (FBS), 2% glutamine, 1% β-fibroblast growth factors (FGF), and 1% streptomycin/amphotericin B (Gibco). Cells were serially passaged using TrypLE Express (Invitrogen) when at

80% confluency. At passage 4, $3{\cdot}10^5$ hBM-MSCs were seeded on MHA/Coll. Cells were also cultured on collagen scaffolds (Coll) (n = 8) with regular media (negative controls) or osteogenic media (positive control for osteogenic differentiation) (n = 8). The osteogenic medium was purchased from Gibco and used according to the protocols of the manufacturers. Medium change was performed every three days.

2.8. Imaging of the 3D cultures

At 3 weeks, the 3D cultures (n = 3) were imaged by a A1 confocal laser microscope (Nikon) and SEM. Cell distribution was assessed by confocal laser microscopy; the cells were fixed with 4% paraformaldehyde (R&D Systems) and then stained with DRAQ5™ (Thermo Fisher), as per manufacturer's protocol. The scaffolds were visualized in the 4′,6-diamidino-2-phenylindole (DAPI) field (350 nm), where they are intrinsically autofluorescent. Images were analyzed with the software NIS Elements (Nikon).

The morphology of the cells was evaluated by SEM. For SEM imaging; cells were fixed with 2.5% glutaraldehyde (Electron Microscopy Science) and then dehydrated in increasing concentrations of ethanol, up to 100%, then vacuum dried [32]. Before imaging, the samples were sputter coated with 9 nm of Pt/Pb, and imaged at 10 kV. The amount of *de novo* calcium phosphate phase produced by the hBM-MSCs was quantified by EDS analysis. The overall amount of Ca, Mg, and P was quantified at 3 weeks of culture.

Data were normalized to the amount of Ca, Mg, and P found in both cell-free Coll and MHA/Coll scaffolds (n = 3).

2.9. Gene expression analysis

The gene expression of selected osteogenic marker genes and of the magnesium transporter 1 (MAGT1) and transient receptor potential cation channel subfamily M member (7TRPM7) (listed in Table S1 of the Supplementary Information) was assessed by q-PCR, for hBM-MSCs cultured *in vitro* on MHA/Coll or Coll (CTRL), after 1 and 3 weeks of culture, as described in paragraph 2.7.

The MHA/Coll specimens harvested from the rabbits at 6 weeks were designated to quantitative - polymerase chain reaction (q-PCR) analysis (n = 8) and compared with specimens of native rabbit transverse process bone, used as control. Both scaffolds and tissue specimens were embedded in 1 mL of Trizol reagent (Life Technologies), homogenized and the RNA extracted with a RNeasy column (Qiagen), as per the manufacturer's protocol. RNA concentration and purity were measured using a NanoDrop ND1000 spectrophotometer (NanoDrop Technologies). The cDNA was synthesized from 1000 ng of total of RNA, using the iScript retrotranscription kit (Bio-Rad Laboratories). Transcribed products were analyzed using Taqman fast advanced master mix (ThermoFisher Scientific) and the appropriate target probes (Supplementary Table S1, ThermoFisher Scientific) on a StepOne Plus real-time PCR system (Applied Biosystems).

2.10. Rabbit bone orthotopic model

To assess MHA/Coll integration and follow bone regeneration, MHA/Coll was implanted unilaterally in rabbit, and bone formation was evaluated at 6 weeks, as previously described [33], through a modified spinal fusion procedure described elsewhere [34,35]. All animal work was approved and supervised by the Houston Methodist Research Institute (HMRI) Institutional Animal Care and Use Committee (IACUC, AUP-0115-002) and guidelines from the American Association for Laboratory Animal Science as well as animal care procedures outlined by the National Institute of Health (NIH) Guide for the Care and Use of Laboratory Animals and were strictly enforced. Scaffolds (4 cm × 1 cm) were sterilized in an AN74ix ethylene oxide chamber (Andersen, Haw River, North Carolina). New Zealand white rabbits (n = 12, Charles River Labs, Houston, Texas) weighing 4.0–5.0 kg each underwent a 72-h acclimation period upon arrival before being housed individually in cages and allowed weight-bearing ambulation, food/water ad libitum, and a tasteless aqueous antibiotic solution (penicillin) for infection prophylaxis. Under the effects of ketamine, midazolam, and inhaled isoflurane anesthesia, a dorsal midline incision approximately 10 cm in length was made directly over palpable spinous processes of the lumbar spine through the skin and subcutaneous tissues. Next, bilateral 6-cm incisions were made just lateral to the palpable mammary bodies from the level of the L4 vertebra to the L7 vertebra. Using blunt dissection between the longissimus, multifidus, and ileocostalis muscles, the transverse processes (TPs) of L5-L6 were exposed and cleaned of thin muscular attachments using a molt-style periosteal elevator. Extra care was taken during dissection near the superior edge of the TP–vertebral body (VB) junction, where the neurovascular bundle exits the spinal canal. Each TP and adjoining intertransverse VB portion was decorticated using a high-speed cone burr until punctate bleeding from the marrow space was encountered. A 1 × 3 cm MHA/Coll was placed between the decorticated TPs on the experimental anatomical right side, functioning in effect to bridge the defect; meanwhile, the anatomical left side was used as an internal control, receiving decortication alone. Incisions were approximated with suture, and after 6 weeks *in vivo*, animal subjects were euthanized by carbon dioxide inhalation, for harvest of the biomaterial samples. No animals suffered any unforeseen morbidity or mortality requiring removal from the study.

2.11. DynaCT scan and measurements of trabecular and cortical bone mass

Under the effect of sedation, lumbosacral computed tomography (DynaCT) scans were acquired for all animals (n = 12) at 24 h, 2, 4, and 6 weeks after implantation, with an Axiom Artis C-arm (d)FC (Siemens Healthcare). Scanning was performed with a 48 cm × 36 cm flat-panel integrated detector. Acquisition parameters for DynaCT were as follows: 70 kV tube voltage, automatic tube current of 107 mA, 20 s scan. Each scan entailed 222° of rotation, with 1 image taken every 0.5° for a total of 444 images (each digital acquisition had a matrix of 514 × 514 pixels) per acquisition. Three-dimensional rendering was obtained through the Inveon Research Workplace 4.2 Software (Siemen Medical Solution Inc.). All DynaCT imaging files were processed and analyzed using Siemens' Inveon Research Workplace. Two regions of interest (ROIs) of identical dimensions were created. One on each surgical side, these ROIs defined the area of analysis to each side of our sample. Utilizing the Hounsfield unit values for tissue densities [36,37], we were able to establish a range that helped us determine the bone volume defined by our ROI. The values used as the minimum threshold to quantify trabecular and cortical bone were the following: for trabecular bone (TB)-like tissue density, the value used was >200HU. For measurement of cortical bone-like tissue density, the units value was >500HU. The quantifications obtained in each study subject were compared with the decorticated control side. *De novo* bone mass was calculated as the difference between the quantification at decorticated and scaffold for bone density corresponding to 200HU and 500HU, respectively.

2.12. Bone histomorphometry

The implant was isolated from the proximal and distal ends of the spine using two axial cuts. The sample was then cut sagittally using the spinal canal as our center point. Afterward, each half was dehydrated and infiltrated and embedded with acrylic resin. Sections were created using the cut and grind technique with the EXAKT Cutting and Grinding System (5–10 μm sections at 500 μm between each level). Sections were stained with Von Kossa/MacNeal's Tetrachrome, Goldner's Trichrome, and hematoxylin and eosin staining (n = 4).

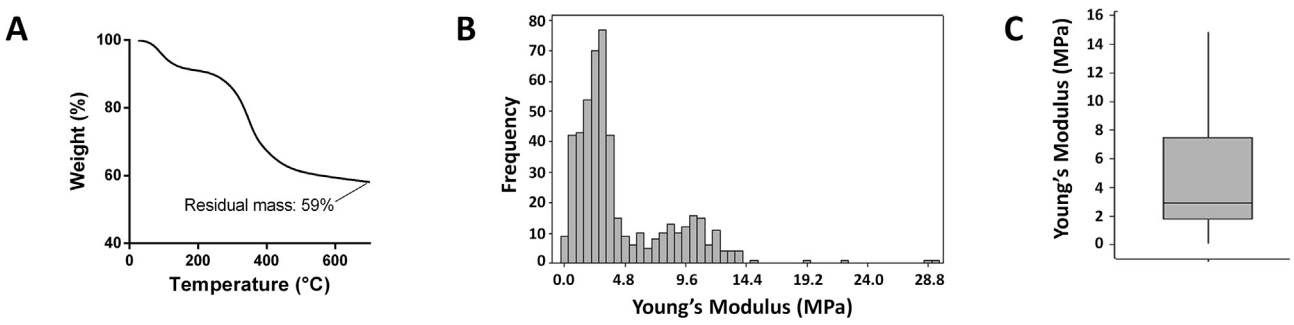

Fig. 1. (A) Representative TGA analysis of the mineral content of MHA/Coll and (B) Young's Modulus measurements. TGA, thermal gravimetric analysis; MHA/Coll, magnesium-doped hydroxyapatite/type I collagen.

2.13. Statistical analysis

All experiments were performed at least in triplicates (for the exact number of replicates, see specific paragraphs). The statistical analysis was performed through the software Prism GraphPad. A one-way analysis of variance (ANOVA) with a post-hoc unpaired *t*-test was used. Data

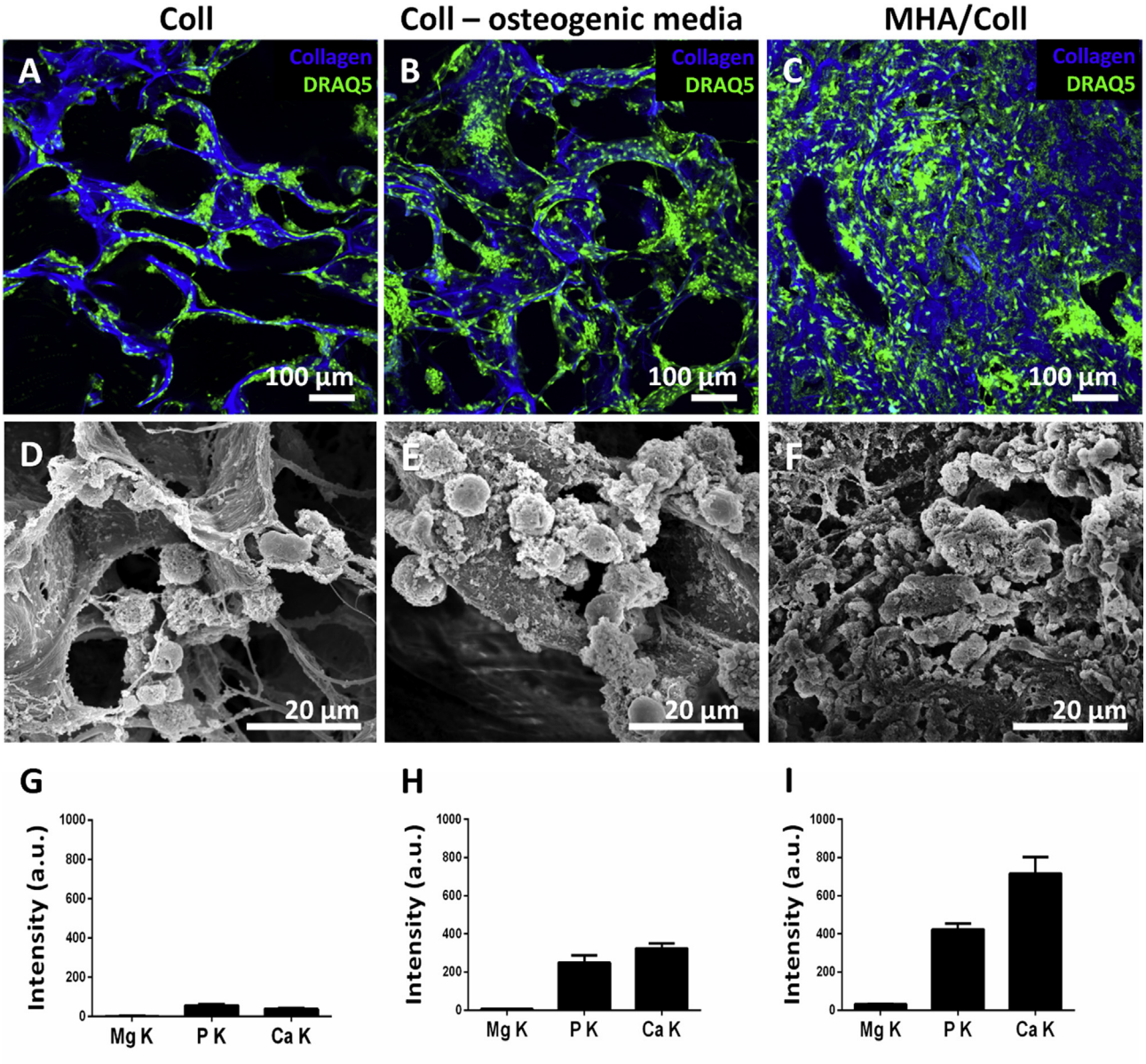

Fig. 2. Confocal laser microscopy and SEM images of hBM-MSCs (green) cultured on Coll, Coll in osteogenic media and MHA/Coll, at 3 weeks (A-C and D-F, respectively). Relative amount (intensity) of magnesium, phosphate and calcium in the scaffolds, for the three corresponding experimental groups, quantified by EDS analysis. Data are normalized to cell-free Coll and MHA/Coll scaffolds, as baselines. SEM, scanning electron microscopy; hBM-MSC, human bone marrow-derived mesenchymal stem cell; MHA/Coll, magnesium-doped hydroxyapatite/type I collagen.

are presented as mean ± standard deviation. For all experiments, * was used for $p < 0.05$, ** for $p < 0.01$, and *** for $p < 0.001$, and **** for $p < 0.0001$.

3. Results

3.1. Characterization of MHA/Coll

The structure of MHA/Coll was evaluated by SEM (Fig. S1). The high-magnification SEM micrographs showed the highly fibrous structure of the composite (Fig. S1A), where the collagen fibers resulted fully mineralized with an amorphous mineral phase (Fig. S1B). The porosity of MHA/Coll was assessed at 70% (±2.1), compared with the 84% (±9) of a non-mineralized scaffold (Fig. S2).

Elemental analysis of MHA/Coll was performed using EDS, where a Ca/P ratio of 1.5 (±0.03) was observed (Fig. S1C). EDS mapping assessed the homogenous distribution of all evaluated elements, within the analyzed areas (Fig. S3). The interaction between MHA and the collagen fibers on which it was nucleated was assessed by FTIR spectroscopy (Fig. S1D). In MHA/Coll, a shift from 1340 to 1337 cm^{-1} in the band corresponding to the stretching of -COO^- group of collagen was observed, because of its interaction with the positively charged MHA nanocrystals. The peak at 872 cm^{-1} in MHA/Coll reveals that the MHA nucleated on the collagen was carbonated, as well as in the MHA powder (Fig. S4).

TGA was performed to assess the extent of mineral phase nucleated on type I collagen. An approximate 40% loss of MHA/Coll initial weight was found, indicating an approximate 60% of actual mineral phase content within the composite (Fig. 1A). AFM analysis was performed on MHA/Coll, to evaluate its elastic properties (Fig. 1B). A total of 521 Young's modulus values were considered, from a minimum of three scaffolds which were prepared independently, demonstrating the robustness of the fabrication technique. While the data set presented an overall Young's modulus close to 6 MPa, a wide range of scaffold stiffness data was observed, as shown in Fig. 1B, with two distinct peaks of Young's

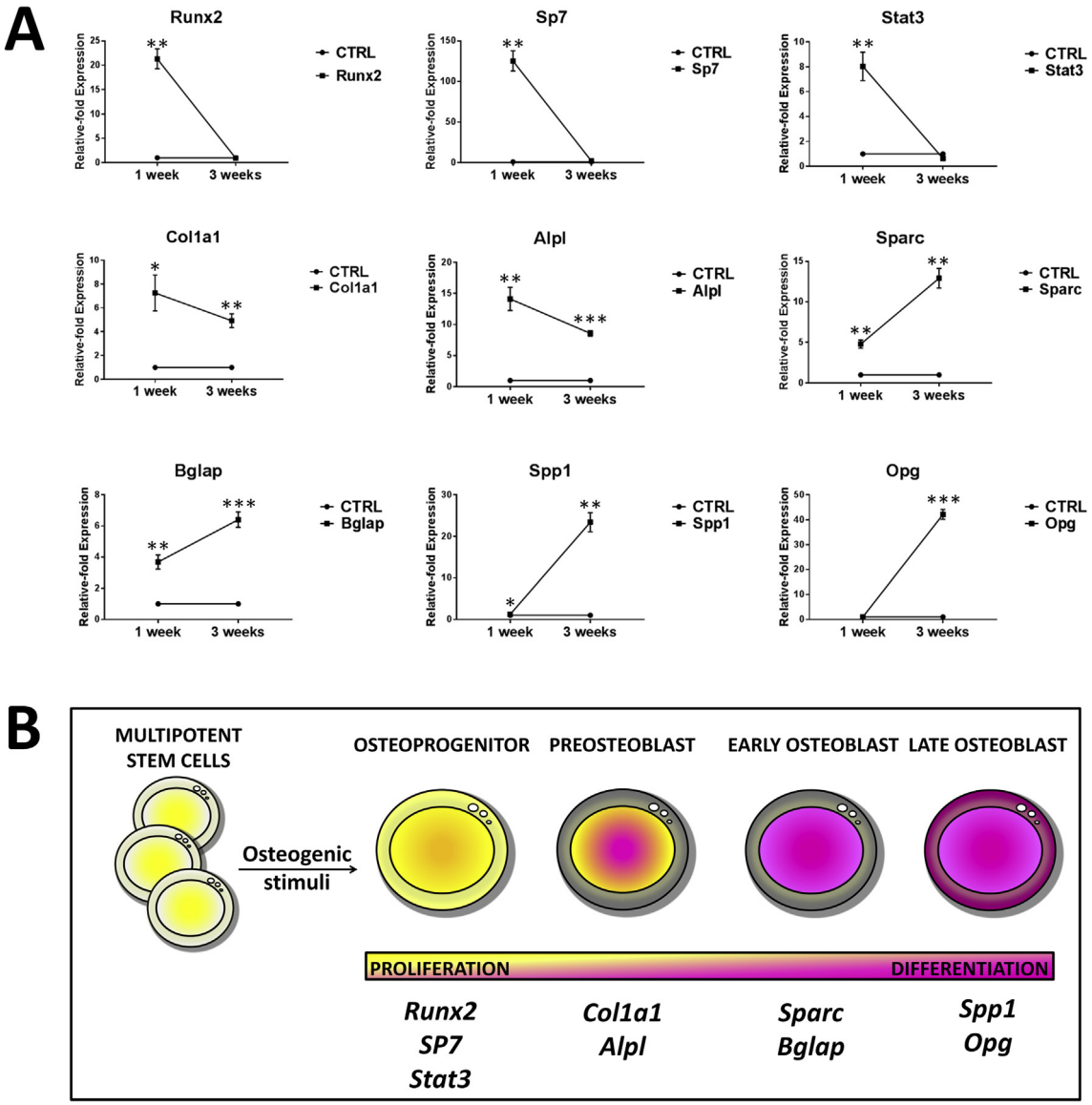

Fig. 3. (A) Relative-fold expression of osteoprogenitor, preosteoblast, and early and late osteoblast marker genes at 1week and 3 weeks of *in vitro* culture of hBM-MSCs cultured on MHA/Coll and control Coll scaffolds. Results were first normalized to the expression of the housekeeping gene GAPDH and then expressed as "relative-fold expression" in comparison to the expression level of the same gene from the CTRL (Coll). Values are reported as mean ± standard deviation. A value of $p < 0.05$ was considered statistically significant: *$p < 0.05$, **$p < 0.01$, ***$p < 0.001$. (B) Schematic representing the different stages of osteogenic differentiation of mesenchymal stem cells, with associated relevant marker genes. hBM-MSC, human bone marrow-derived mesenchymal stem cell; MHA/Coll, magnesium-doped hydroxyapatite/type I collagen.

Modulus, representing more elastic collagen areas and those that were significantly stiffer or less elastic. The first distribution peak, comprising all data points between 0.1 and 5 MPa and including 70% of the total data set, exhibited an elastic modulus of 2.35 ± 1.16 MPa. These areas were interspersed with stiffer areas of the second peak, which comprised 30% of the total data set and exhibited a range between 5.5 and 14 MPa, with an average Young's modulus of 9.52 ± 2.10 MPa. The raw data are reported in Table S2.

3.2. In vitro test of MHA/Coll with hBM-MSCs

After 3 weeks of culture, hBM-MSCs-MHA/Coll constructs were imaged by confocal laser microscopy to assess their overall morphology and cell distribution. Cells cultured on Coll in regular media, used as controls, resulted organized along the walls of the scaffold pores, and the scaffold itself was found highly porous (Fig. 2A).

Cells cultured on Coll in osteogenic media were found organized in bigger clusters, within and along the pore walls (Fig. 2B). MHA/Coll samples displayed a completely different morphology (Fig. 2C). The scaffold appeared denser and less porous, with cells organized in big clusters within the pores. These observations were further confirmed by the SEM micrographs. Cells on Coll (regular media and osteogenic media) were easily identified, along the pores of the scaffold (Fig. 2D and E), whereas the cells on MHA/Coll appeared embedded within the amorphous mineral phase/collagen matrix of the scaffold and were hardly identifiable (Fig. 2F). EDS analysis was also performed on these samples to assess the deposition of mineral phase by the hBM-MSCs and its eventual elemental composition (Fig. 2G, H, I). In all samples, some extent of mineralization was found, but the most significant amount of *de novo* mineralization was found in the MHA/Coll experimental group.

3.3. In vitro osteogenic differentiation of hBM-MSCs

We identified a comprehensive panel of osteogenic marker genes and monitored their dynamic expression at early and late differentiation stages (1 week and 3 weeks, respectively) for hBM-MSCs cultured on MHA/Coll and Coll scaffolds (used as controls). For cells cultured on MHA/Coll, we observed a notable induction of osteoprogenitor marker genes and early osteoblast (OB) marker genes at 1 week and a less pronounced increase in their expression at 3 weeks; whereas late OB marker genes and osteocyte marker genes resulted expressed at a higher level at 3 weeks (Fig. 3, and summary of data and their statistical significance in Table 1).

3.4. In vitro expression of MAGT1 gene by hBM-MSCs

Considering the presence of calcium and magnesium in the formulation of our MHA/Coll, we investigated the *in vitro* expression of genes MAGT1 and TRPM7. MAGT1 was found significantly overexpressed at both experimental time points of 1 week ($p < 0.001$) and 3 weeks ($p < 0.05$), when hBM-MSCs were cultured on MHA/Coll, compared with the CTRL (Coll) (Fig. 4). MAGT1 was found expressed at a higher level at 1 week than 3 weeks. TRPM7 was found to be not overexpressed at neither time points, compared with the CTRL (data not shown).

3.5. Orthotopic de novo bone formation

Operatively, MHA/Coll was found easy to handle. When explanted, the implants were found significantly hardened and bone-like in appearance. Boney transformation of scaffolds was monitored by DynaCT (Fig. 5A–C), at 2, 4 and 6 weeks, and finally evaluated by histology at 6 weeks (Fig. 6). Compared with the decorticated side alone, there was significant mineral deposition. While no difference in TB formation was seen over time, the mean bone mass at 200HU decreased over time. Conversely increases in the mass of bone measured at 500HU and associated with cortical bone was seen at 4 weeks and 6 weeks compared with the 2-week time point (Fig. 5D). Mean *de novo* bone formation increased from week 2 (152.1 ± 38.2 mm^3) to week 4 (293.9 ± 122.4 mm^3) ($p < 0.05$). This significant increase in the cortical fraction of newly formed bone continued into week 6 (256.2 ± 55.6 mm^3). From week 2 to week 4, the cortical fraction of bone nearly doubled. Overall, more TB was measured compared with cortical bone.

At 6 weeks, histology confirmed the formation of an extended mass of bone-like tissue within the implants. A significant amount of mineral phase was found in MHA/Coll samples evaluated through Von Kossa stain, on non-decalcified tissue slices. The staining resulted of similar intensity to TB, used as control (Fig. 6A and B), and the osteoid portion of the tissue was clearly distinguishable, although it appeared not fully remodeled at this time point, compared with vertebral bone. Similarly, Goldner's Trichrome staining of MHA/Coll samples allowed to clearly discriminate between mineralized bone matrix (mineral phase—MP) and osteoids, where OB and osteoclasts (OC) were both identified (Fig. 6C and D). Finally, hematoxylin and eosin staining confirmed the presence of OCs and OBs in the osteoid area of MHA/Coll samples, similarly to the control TB specimens (Fig. 6E and F).

3.6. In vivo osteogenesis

We assessed the stage of remodeling of the newly formed bone-like

Table 1
Relative-fold expression of osteoprogenitor, early and late osteoblast, and osteocyte marker genes at 1 week and 3 weeks for hBM-MSCs cultured on MHA/Coll and control Coll scaffolds.

Gene	Relative-fold expression	
	1 week	3 weeks
Osteoprogenitor marker genes:		
RUNX2	21.33 ± 2.03 ($p < 0.01$)	0.95 ± 0.12
SP7	125.35 ± 12.42 ($p < 0.01$)	2.19 ± 0.25 ($p < 0.05$)
STAT3	8.03 ± 1.14 ($p < 0.01$)	0.64 ± 0.03
Early osteoblast marker genes:		
COL1A1	7.26 ± 1.51 ($p < 0.05$)	4.93 ± 0.58 ($p < 0.01$)
ALPL	14.11 ± 1.85 ($p < 0.01$)	8.58 ± 0.44 ($p < 0.001$)
Late osteoblast marker genes:		
SPARC	4.81 ± 0.50 ($p < 0.01$)	12.92 ± 1.21 ($p < 0.01$)
BGLAP	3.69 ± 0.45 ($p < 0.01$)	6.41 ± 0.49 ($p < 0.001$)
Osteocyte marker genes:		
SPP1	1.23 ± 0.16 ($p < 0.05$)	23.41 ± 2.30 ($p < 0.01$)
OPG	1.03 ± 0.07	42.16 ± 1.98 ($p < 0.001$)

hBM-MSC, human bone marrow-derived mesenchymal stem cell; MHA/Coll, magnesium-doped hydroxyapatite/type I collagen.

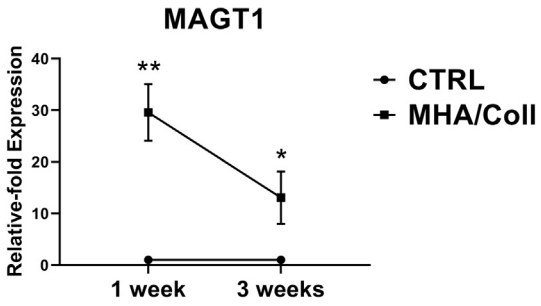

Fig. 4. Relative-fold expression of MAGT1 at 1week and 3 weeks of *in vitro* culture of hBM-MSCs cultured on MHA/Coll and Coll (CTRL). TRPM7 was not found expressed at neither time points (data not shown). Results were first normalized to the expression of the housekeeping gene GAPDH and then expressed as "relative-fold expression" in comparison to the expression level of the same gene from the CTRL. Values are reported as mean ± standard deviation. A value of $p < 0.05$ was considered statistically significant: *$p < 0.05$, **$p < 0.01$. hBM-MSC, human bone marrow-derived mesenchymal stem cell; MHA/Coll, magnesium-doped hydroxyapatite/type I collagen; MAGT1, magnesium transporter 1.

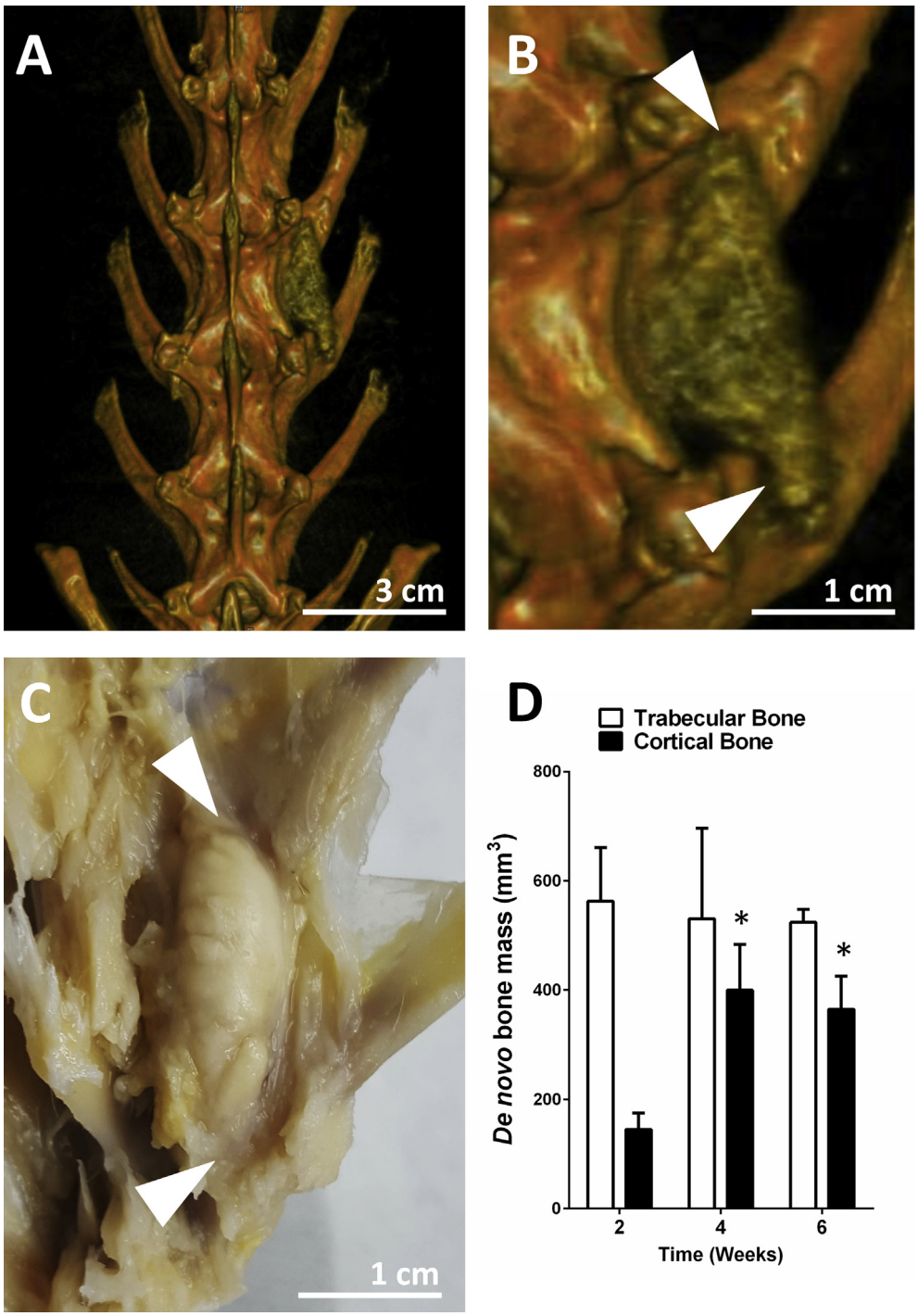

Fig. 5. 3D rendering obtained by DynaCT scan of a representative spine showing radiologic bone mass formation in correspondence of the scaffold (arrowhead) (A, B). Bone-like scaffold at 6 weeks, upon retrieval, showing integration with surrounding tissue (arrowhead) (C). MHA/Coll allowed early and robust trabecular bone formation as well as cortical bone ingrowth as early as 2 weeks (D).

mass through q-PCR. Regarding the expression levels of the selected osteogenesis-associated marker genes, DLX5 (BMP-responsive transcriptional activator) was the only gene that was not overexpressed in the newly formed bone-like mass within the scaffold, compared with TP bone (not statistically significant), whereas the expression level of the remaining early and late osteogenesis-associated marker genes was significantly higher compared with the control (TP bone) (RUNX2 2.21 $\pm$ 0.24 ($p < 0.05$), COL1A1 2.28 $\pm$ 0.16 ($p < 0.05$), SPARC 3.19 $\pm$ 0.07 ($p < 0.01$), and SPP1 3.67 $\pm$ 0.09 ($p < 0.001$)) (Fig. 7). The significant overexpression of SPARC and SPP1, which are markers for late OBs and osteocytes, are evidence that bone maturation on the scaffold initiated at only 6 wks.

The selected bone marrow stromal cell–associated marker genes were expressed in the newly formed bone-like mass generated by MHA/Coll, but their level of expression was lower compared towith the control. Only VCAM1, which is usually downregulated during hematopoietic progenitor cell mobilization, was found overexpressed 1.95 $\pm$ 0.25-fold compared with TP bone, suggesting newly developed hematopoietic stem cells (HSCs) had low migration activity at 6 weeks. CD38, SELE, and KDR, which are key HSCs surface markers, were found expressed in the newly

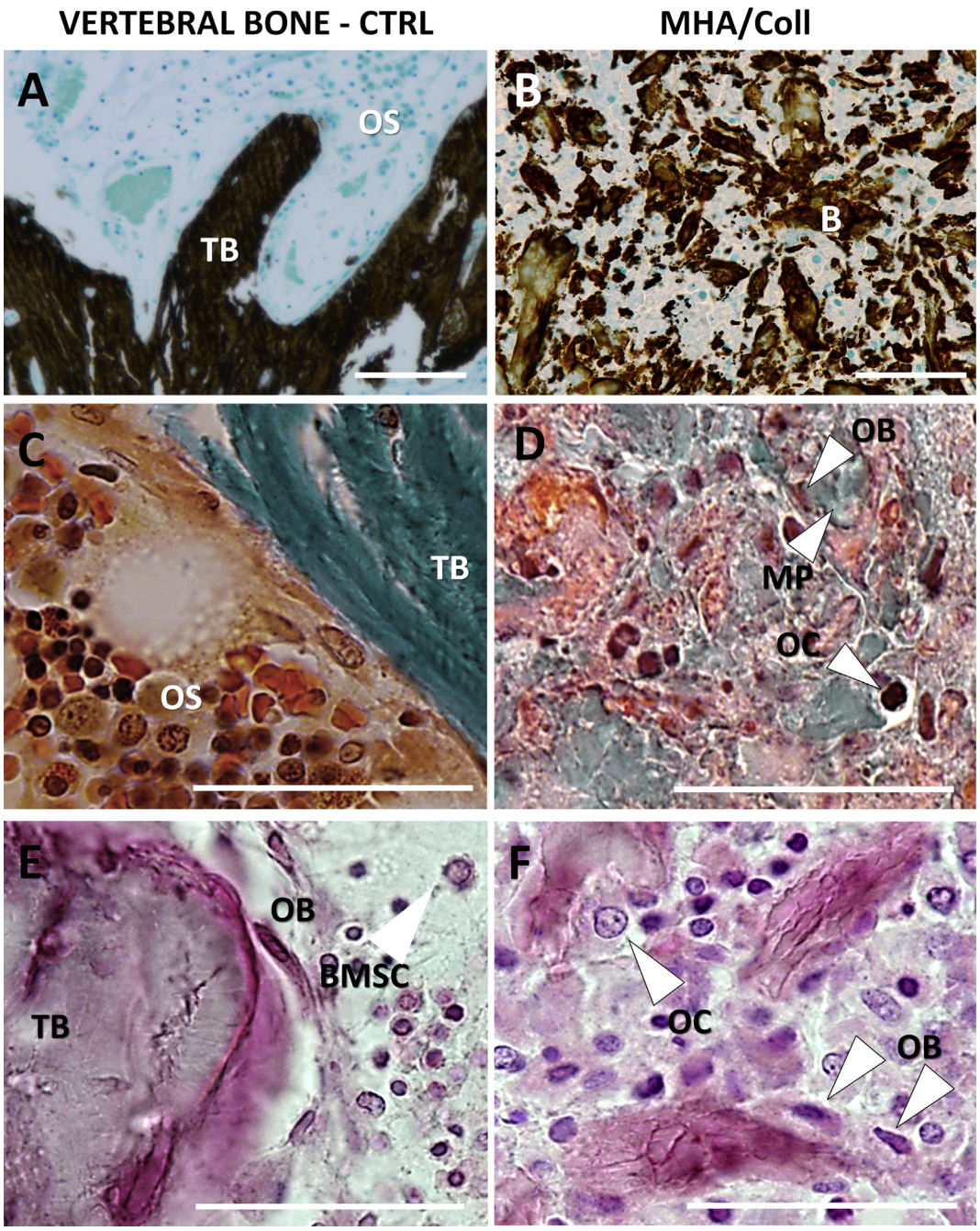

Fig. 6. Von Kossa (A, B), Goldner's Trichrome (C, D), and hematossilin-eosin (E, F) staining of non-demineralized vertebral trabecular bone and MHA/Coll specimens at 6 weeks, respectively. TB, trabecular bone; OS, osteoid; MP, mineral phase; OB, osteoblast; OC, osteoclast; BMSC, bone marrow stem cell.

formed bone mass within the scaffold, at levels slightly lower than that of TP bone (0.54 ± 0.15, 0.51 ± 0.04 *$p < 0.05$ and 0.61 ± 0.02 **$p < 0.01$, respectively) (Fig. 6). Similarly, all selected bone marrow stromal cells marker genes were found expressed, but at slightly lower levels than those of the control (ALCAM: 0.39 ± 0.02, ITGB1: 0.73 ± 0.03, and VIM: 0.72 ± 0.06), with an overall expression level of 39%, 73%, and 72%, respectively, when compared with native bone.

4. Discussion

Regenerative bone tissue engineering encompasses a wide range of different strategies, materials, and biologics aimed at regenerating bone [38]. Owing to the varying types and functions of bone tissue, there is no universal approach to bone tissue engineering; and scaffolds, for example, are required to be tailored to specific design and mechanical strength requirements, depending on location and microscale architecture of specific bones [39]. Although the use of BMP-2 allowed for bone regeneration in multiple clinical settings, the severe side-effects associated with high dosing discouraged many orthopedic surgeons from using it. Thus, a fully biocompatible and biodegradable device, able to induce bone formation without the use of recombinant growth factors or any other exogenous biologics, would significantly benefit the current standard of care for bone regeneration [28]. In the present work, we investigated the osteogenic potential of a biomimetic hybrid composite—MHA/Coll—demonstrating its ability to support the formation of newly formed bone-like tissue in a large orthotopic model, within only 6 weeks from implantation, without the use of any exogenous biologics.

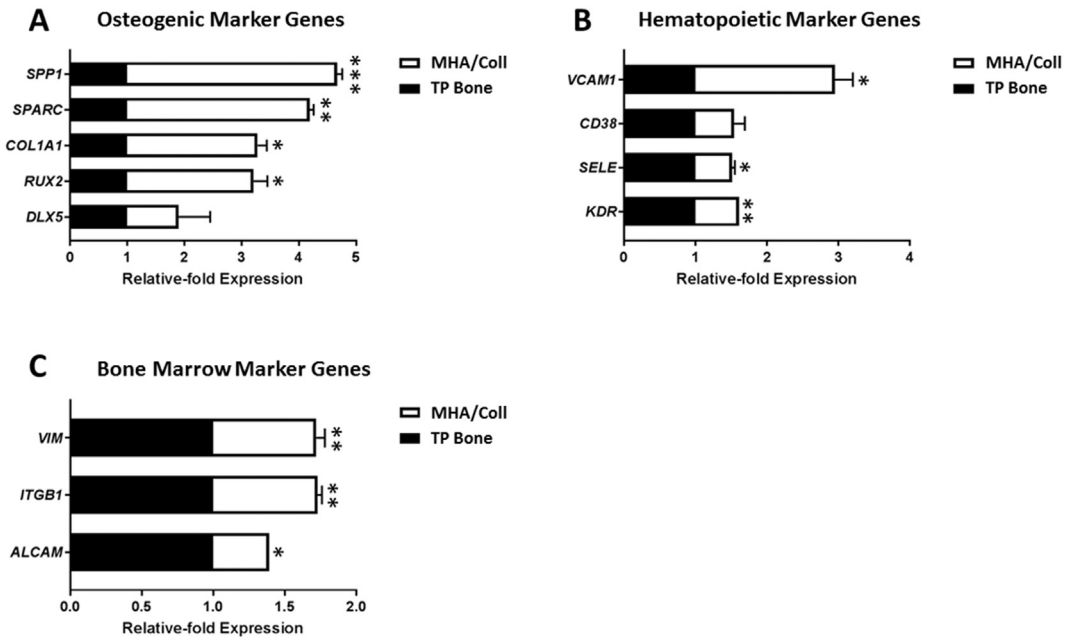

Fig. 7. Releative-fold Expression of osteogenic (A), hematopoitic (B), and bone marrow–associated marker genes (C) detected for MHA/Coll group at 6 weeks after implantation in the orthotopic model in rabbit, compared with naïve spinal bone. Results were first normalized to the expression of the housekeeping gene GAPDH and then expressed as "relative-fold expression" in comparison to the expression level of the same gene from the CTRL. Values are reported as mean ± standard deviation. A value of $p < 0.05$ was considered statistically significant: *$p < 0.05$, **$p < 0.01$, ***$p < 0.001$. TP, transverse process; MHA/Coll, magnesium-doped hydroxyapatite/type I collagen.

Regenerating bone is characterized by the presence of woven, or immature bone, with Young's moduli that range from 30 to 1000 MPa depending on the distance from the fracture point, with an average of around 13 MPa [40]. Nanocrystalline apatites have been successfully substituted with a variety of ions, to reach increasing degrees of biomimicry to the composition of the bone mineral phase [41]. However, devices fabricated with these biomimetic apatites lack in recapitulating other vital features of bone, such as its architecture and mechanical properties. Synthetic and natural polymers have been combined with nanoapatites to create loosely packed fibrous meshes that have a much lower stiffness and facilitate cellularization and encourage new tissue formation by progenitor and bone cells [42]. Our MHA/Coll scaffold was synthesized through an innovative biologically inspired synthetic process, which was demonstrated to recapitulate the main steps of bone biomineralization [28]. Similarly to the biomineralization process of the bone, the organic template on which the biomimetic apatite is nucleated plays a crucial role. In fact, during the synthesis, type I collagen allows for the structural and morphological control over the growth of the apatite crystals, leading to a nanoscopic and microscopic architecture similar to that found in human bone [28,43]. During the pH-driven self-assembly of the organic template, the mineral phase is synthesized and nucleated directly on the collagen fibers. This resulted in a composite material (Figs. S1A and B), with unique chemical, morphological, and mechanical cues, known to be crucial in guiding cell recruitment and migration [28]. Previous nanostructural analysis of single-collagen bundles showed that MHA was homogenously nucleated along the collagen bundles, overall increasing their roughness when compared with unmineralized collagen fibers [28]. Herein, for the first time, we have assessed the nanomechanics of these collagen fibers in situ, within the gross 3D MHA/Coll scaffold construct compared to bone, by nanoindentation or force volume mapping. MHA/Coll demonstrated Young's modulus of less than 100 MPa and was not matched specifically to the stiffness of immature bone (Fig. 1). It is well known that cells are able to sense and voluntarily migrate along gradients of stiffness within a material (durotaxis) [44]. In our study, hBM-MSCs underwent osteogenic differentiation when seeded on MHA/Coll *in vitro*, and host's cells sequestered retain an osteogenic genotype and phenotype *in vivo*, which may suggest that a softer highly biomimetic material, where progenitor and somatic cells experience a relatively low stiffness, could be more conducive for new tissue formation. Thus, the gradients of varying nanomechanical properties observed may have contributed to enhanced cell ingrowth, providing a niche for such osteogenic differentiation and subsequent repair. This is further supported by the efficient osteodifferentiation of hBM-MSCs and their *de novo* mineral deposition characterized *in vitro* (Fig. 2), and of new bone formation characterized *in vivo* by DynaCT scan and histology (Figs. 5 and 6 respectively).

We had previously found that hBM-MSCs upregulated OB-associated marker genes when cultured on MHA/Coll, *in vitro* [28]. Interestingly, in the present study, a more thorough osteogenesis-associated gene expression analysis revealed that hBM-MSCs had sequentially upregulated all the key marker genes of each stage of the osteogenic differentiation and maturation pathway when cultured on MHA/Coll, without any exogenous biologics and in a more efficient fashion than when cultured in osteogenic media (Fig. 3).

Other biomaterials containing magnesium have been proposed for bone regeneration, as they allow for enhanced osteogenesis and increased bone density [45,46], although the mechanisms underlying the biological effects of magnesium are still mostly unveiled [47–51]. Among all, magnesium-based bioceramic phases have been tested because of their superior osteogenic properties, significant bone-like apatite formation ability, and excellent bioactivity [52–54]. Recent findings suggested that the genes MAGT1 and TRPM7 (encoding for the magnesium-selective cation transporter magnesium transporter 1 and the non-magnesium–specific transient receptor potential cation channel subfamily M member 7, respectively) are upregulated and significantly contribute to the orchestration of the osteogenic differentiation of h-MSCs [55]. It was also demonstrated that silencing either one of them hastens the expression of osteogenic markers as well as calcium deposition *in vitro* [55]. Thus, the overexpression of MAGT1, at as early as 1 week of culture on MHA/Coll compared with the control (Fig. 4), would suggest that the composition of MHA/Coll (containing both magnesium and calcium) itself may improve the orchestration of the osteogenic

differentiation of hBM-MSCs, and even more efficiently than osteogenic media. Moreover, similarly to our *in vitro* findings, Castiglioni et al. observed that when TRPM7 is silenced and MAGT1 is upregulated, the osteogenic differentiation of h-MSCs is enhanced and associated with increased calcium deposition [55]. In our study, we found MAGT1 was overexpressed at both 1 and 3 weeks, whereas TRPM7 was downregulated (Fig. 4). This could have enhanced the osteogenic stimulus delivered by the scaffold, through a mechanism similar to that described by Castiglioni et al., which could in part explain the promising results obtained *in vivo* within only 6 weeks from implantation of MHA/Coll in an orthotopic model.

With the highest level of expression of MAGT1 being at the earlier time point *in vitro* (1 week), we hypothesize that this early MAGT1-mediated harmonized osteogenic differentiation of the progenitor cells could explain the significant formation of new bone *in vivo* (Fig. 6). In fact, in the orthotopic model, the scaffold promoted the formation of a significant amount of bone-like mass with density similar to that of TB (>200HU) [37], only 2 weeks after implantation in the orthotopic model. Furthermore, its maturation and densification also initiated at only 2 weeks, as demonstrated by the increasing volume of newly formed bone having density similar to that of cortical bone (>500HU) [37] that accumulated over the weeks (Fig. 4). This represents a significant accomplishment considering it was achieved without the contribution of any heterologous cytokines or engraftment of progenitor cells on the scaffold, before implantation, and correlated with our previous findings [28]. Because the rapid integration and remodeling of a bone scaffold is vital for the ultimate outcome, these results are all the more significant and highlight the enhanced osteoinductive nature of MHA/Coll.

Finally, particularly remarkable of this study was not only the efficient recruitment of progenitor and bone cells *in vivo* (clearly identified by histology and through gene expression, Figs. 5 and 6, respectively), which surely facilitated the formation of bone-like tissue, but also that some of such cells belonged to the hematopoietic lineage. When compared with mature bone (naïve TP bone), the selected hematopoietic-associated and bone marrow stromal cell–associated marker genes displayed a lower level of expression within our scaffold (Fig. 6). However, these results are still very significant as they reveal a developing primitive hematopoietic niche within the newly formed tissue formed by MHA/Coll. It was been recently reported that mesenchymal progenitors are sufficient to create bony ossicles that are populated by host vasculature and hematopoietic stem cells [56,57]. Similarly, our data suggest that MHA/Coll is able to be not only colonized by mesenchymal osteoprogenitors but also by hematopoietic precursors that may contribute to the assembly of a hematopoietic niche, toward a full maturation of the newly deposited bone tissue [56]. Although evaluating the formation of bone marrow was not the main purpose of this study, this data laid the foundation for further investigation of the ability of MHA/Coll to promote the regeneration of functional bone tissue, including a bone marrow niche.

To our knowledge, this study reports for the first time the formation of an extensive mass of TB–like and cortical bone–like tissue within only 6 weeks after implantation, through a biologics-free scaffold, able to support the formation of both an osteogenic and hematopoietic niche.

5. Conclusions

In this study, we reported the enhanced osteoconductive potential of MHA/Coll, a highly biomimetic hybrid composite, based on magnesium-substituted hydroxyapatite and type I collagen, synthesized through a bioinspired mineralization process of type I collagen. We first demonstrated its ability to induce, orchestrate, and harmonize the osteogenic differentiation of hBM-MSCs *in vitro*. Second, the significant new TB and early cortical bone formation at 2 weeks and 4 weeks clearly proved the osteoinductive nature of MHA/Coll. Finally, our findings suggested that the remodeling we observed may involve also the formation of a bone marrow-like niche, which could lead to functional bone tissue regeneration, at longer time points.

Author contributions

S.M., F.T., A.T., B.W., and E.T. conceived the initial idea and designed the study. S.M. fabricated and characterized the scaffolds and performed all *in vitro* assays and microscopy. F.C. and J.V.E. performed the *in vivo* studies and data analysis. X.W. performed the gene expression analysis. S.G. and L.F. performed the nanomechanical analysis. All authors contributed to the data analysis and in drafting the manuscript.

Conflict of interest

The authors declare that they have no known competing financial interests or personal relationships that could have appeared to influence the work reported in this paper.

Acknowledgments

The authors would like to acknowledge Dr. Monica Sandri and Dr. Joseph Fernandez-Moure for their suggestions and troubleshooting. The authors thank Ms. Nupur Basu for her help with the culture of stem cells. The authors acknowledge the HMRI SEM core and HMRI ACTM core. Authors thank the Pre-clinical Catheterization laboratory of HMRI for DynaCT analysis and the Ratliff Histology Consultants, LLC, for processing of the histological specimens. This study was supported by the Brown Foundation, Project ID: 18130011 (E.T.), the Cullen Trust for Health Care Foundation, Project ID: 18130014 (E.T.), the Hearst foundation, Project ID: 18130017 (E.T.), and a pilot project grant by the Department of Orthopedics of the Houston Methodist Hospital (S.M.).

Appendix A. Supplementary data

Supplementary data to this article can be found online at https://doi.org/10.1016/j.mtbio.2019.100005.

References

[1] T. Schubert, S. Lafont, G. Beaurin, G. Grisay, C. Behets, P. Gianello, D. Dufrane, Critical size bone defect reconstruction by an autologous 3D osteogenic-like tissue derived from differentiated adipose MSCs, Biomaterials 34 (18) (2013) 4428–4438.
[2] E.D. Arrington, W.J. Smith, H.G. Chambers, A.L. Bucknell, N.A. Davino, Complications of iliac crest bone graft harvesting, Clin. Orthop. Relat. Res. 329 (1996) 300–309.
[3] R.W. Bucholz, Nonallograft osteoconductive bone graft substitutes, Clin. Orthop. Relat. Res. 395 (2002) 44–52.
[4] J.S. Silber, D.G. Anderson, S.D. Daffner, B.T. Brislin, J.M. Leland, A.S. Hilibrand, A.R. Vaccaro, T.J. Albert, Donor site morbidity after anterior iliac crest bone harvest for single-level anterior cervical discectomy and fusion, Spine 28 (2) (2003) 134–139.
[5] V. Campana, G. Milano, E. Pagano, M. Barba, C. Cicione, G. Salonna, W. Lattanzi, G. Logroscino, Bone substitutes in orthopaedic surgery: from basic science to clinical practice, J. Mater. Sci. Mater. Med. 25 (10) (2014) 2445–2461.
[6] P.V. Giannoudis, H. Dinopoulos, E. Tsiridis, Bone substitutes: an update, Injury 36 (3) (2005) S20–S27.
[7] T.N. Vo, F.K. Kasper, A.G. Mikos, Strategies for controlled delivery of growth factors and cells for bone regeneration, Adv. Drug Deliv. Rev. 64 (12) (2012) 1292–1309.
[8] M. Geiger, R. Li, W. Friess, Collagen sponges for bone regeneration with rhBMP-2, Adv. Drug Deliv. Rev. 55 (12) (2003) 1613–1629.
[9] D. Ben-David, S. Srouji, K. Shapira-Schweitzer, O. Kossover, E. Ivanir, G. Kuhn, R. Müller, D. Seliktar, E. Livne, Low dose BMP-2 treatment for bone repair using a PEGylated fibrinogen hydrogel matrix, Biomaterials 34 (12) (2013) 2902–2910.
[10] G. Grabowski, C.A. Cornett, Bone graft and bone graft substitutes in spine surgery: current concepts and controversies, J. Am. Acad. Orthop. Surg. 21 (1) (2013) 51–60.
[11] E.S. Place, N.D. Evans, M.M. Stevens, Complexity in biomaterials for tissue engineering, Nat. Mater. 8 (6) (2009) 457–470.
[12] E.J. Carragee, G. Chu, R. Rohatgi, E.L. Hurwitz, B.K. Weiner, S.T. Yoon, G. Comer, B. Kopjar, Cancer risk after use of recombinant bone morphogenetic protein-2 for spinal arthrodesis, J Bone Joint Surg Am 95 (17) (2013) 1537–1545.
[13] H.S. Makanji, A. Bhalla, C.M. Bono, BMP-2 with Anterior Lumbar Interbody Fusion: Clinical Usage and Recent Controversies, Semin Spine Surg, Elsevier, 2016, pp. 233–238.
[14] A.I. Caplan, Mesenchymal stem cells: cell–based reconstructive therapy in orthopedics, Tissue Eng. 11 (7–8) (2005) 1198–1211.

[15] W.L. Grayson, B.A. Bunnell, E. Martin, T. Frazier, B.P. Hung, J.M. Gimble, Stromal cells and stem cells in clinical bone regeneration, Nat. Rev. Endocrinol. 11 (3) (2015) 140.
[16] M. Bouyer, R. Guillot, J. Lavaud, C. Plettinx, C. Olivier, V. Curry, J. Boutonnat, J.-L. Coll, F. Peyrin, V. Josserand, Surface Delivery of Tunable Doses of BMP-2 from an Adaptable Polymeric Scaffold Induces Volumetric Bone Regeneration, Biomaterials, 2016.
[17] S.S. Lee, T. Fyrner, F. Chen, Z. Álvarez, E. Sleep, D.S. Chun, J.A. Weiner, R.W. Cook, R.D. Freshman, M.S. Schallmo, Sulfated glycopeptide nanostructures for multipotent protein activation, Nat. Nanotechnol. 12 (8) (2017) 821–829.
[18] J.A. Inzana, D. Olvera, S.M. Fuller, J.P. Kelly, O.A. Graeve, E.M. Schwarz, S.L. Kates, H.A. Awad, 3D printing of composite calcium phosphate and collagen scaffolds for bone regeneration, Biomaterials 35 (13) (2014) 4026–4034.
[19] J. Zhang, S. Zhao, Y. Zhu, Y. Huang, M. Zhu, C. Tao, C. Zhang, Three-dimensional printing of strontium-containing mesoporous bioactive glass scaffolds for bone regeneration, Acta Biomater. 10 (5) (2014) 2269–2281.
[20] N. Sachot, O. Castaño, M.A. Mateos-Timoneda, E. Engel, J.A. Planell, Hierarchically engineered fibrous scaffolds for bone regeneration, J. R. Soc. Interface 10 (88) (2013) 20130684.
[21] S. Bose, M. Roy, A. Bandyopadhyay, Recent advances in bone tissue engineering scaffolds, Trends Biotechnol. 30 (10) (2012) 546–554.
[22] W. Wang, K.W.K. Yeung, Bone grafts and biomaterials substitutes for bone defect repair: a review, Bioactive Materials 2 (4) (2017) 224–247.
[23] E. Gallazzi, N. Logoluso, E.V. De, L. Drago, Antibiotic-loaded regenoss for the treatment of septic bone defects: in vitro study and preliminary clinical experience, J. Biol. Regul. Homeost. Agents 29 (4 Suppl) (2015) 103–110.
[24] M. Mozzati, G. Gallesio, G. Staiti, G. Iezzi, A. Piattelli, C. Mortellaro, Socket preservation using a biomimetic nanostructured matrix and atraumatic surgical extraction technique, J. Craniofac. Surg. 28 (4) (2017) 1042–1045.
[25] R.Y. Basha, M. Doble, Design of biocomposite materials for bone tissue regeneration, Mater. Sci. Eng. C 57 (2015) 452–463.
[26] B. Grigolo, P. Dolzani, C. Giannetti, M. Tenucci, G. Calvosa, Case Report Use of a fully-resorbable, biomimetic composite hydroxyapatite as bone graft substitute for posterolateral spine fusion: a case report, Int. J. Clin. Exp. Med. 9 (11) (2016) 22458–22462.
[27] H. Cölfen, Bio-inspired Mineralization Using Hydrophilic Polymers, Biomineralization II, Springer, 2006, pp. 1–77.
[28] S. Minardi, B. Corradetti, F. Taraballi, M. Sandri, J. Van Eps, F.J. Cabrera, B.K. Weiner, A. Tampieri, E. Tasciotti, Evaluation of the osteoinductive potential of a bio-inspired scaffold mimicking the osteogenic niche for bone augmentation, Biomaterials 62 (2015) 128–137.
[29] A. Tampieri, S. Sprio, M. Sandri, F. Valentini, Mimicking natural bio-mineralization processes: a new tool for osteochondral scaffold development, Trends Biotechnol. 29 (10) (2011) 526–535.
[30] S. Sprio, M. Sandri, M. Iafisco, S. Panseri, A. Adamiano, M. Montesi, E. Campodoni, A. Tampieri, Bio-inspired assembling/mineralization process as a flexible approach to develop new smart scaffolds for the regeneration of complex anatomical regions, J. Eur. Ceram. Soc. 36 (12) (2016) 2857–2867.
[31] S. Minardi, M. Sandri, J.O. Martinez, I.K. Yazdi, X. Liu, M. Ferrari, B.K. Weiner, A. Tampieri, E. Tasciotti, Multiscale Patterning of a Biomimetic Scaffold Integrated with Composite Microspheres, Small, 2014.
[32] S. Minardi, B. Corradetti, F. Taraballi, M. Sandri, J.O. Martinez, S.T. Powell, A. Tampieri, B.K. Weiner, E. Tasciotti, Biomimetic Concealing of PLGA Microspheres in a 3D Scaffold to Prevent Macrophage Uptake, Small, 2016.
[33] J.M. Cottrell, M.C. van der Meulen, J.M. Lane, E.R. Myers, Assessing the stiffness of spinal fusion in animal models, HSS J. 2 (1) (2006) 12–18.
[34] S.D. Boden, J.H. Schimandle, W.C. Hutton, An experimental lumbar intertransverse process spinal fusion model: radiographic, histologic, and biomechanical healing characteristics, Spine 20 (4) (1995) 412–420.
[35] M.A. Morone, S.D. Boden, Experimental posterolateral lumbar spinal fusion with a demineralized bone matrix gel, Spine 23 (2) (1998) 159–167.
[36] M.R. Norton, C. Gamble, Bone classification: an objective scale of bone density using the computerized tomography scan, Clin. Oral Implant. Res. 12 (1) (2001) 79–84.
[37] R.C.G. de Oliveira, C.R. Leles, L.M. Normanha, C. Lindh, R.F. Ribeiro-Rotta, Assessments of trabecular bone density at implant sites on CT images, Oral Surg. Oral Med. Oral Pathol. Oral Radiol. Endod. 105 (2) (2008) 231–238.
[38] X. Yu, X. Tang, S.V. Gohil, C.T. Laurencin, Biomaterials for bone regenerative engineering, Adv. Healthc. Mater. 4 (9) (2015) 1268–1285.
[39] D.W. Hutmacher, J.T. Schantz, C.X.F. Lam, K.C. Tan, T.C. Lim, State of the art and future directions of scaffold-based bone engineering from a biomaterials perspective, J. Tissue Eng. Regenerat. Med. 1 (4) (2007) 245–260.
[40] P. Leong, E. Morgan, Measurement of fracture callus material properties via nanoindentation, Acta Biomater. 4 (5) (2008) 1569–1575.
[41] C. Drouet, F. Bosc, M. Banu, C. Largeot, C. Combes, G. Dechambre, C. Estournès, G. Raimbeaux, C. Rey, Nanocrystalline apatites: from powders to biomaterials, Powder Technol. 190 (1) (2009) 118–122.
[42] W.J. Li, C.T. Laurencin, E.J. Caterson, R.S. Tuan, F.K. Ko, Electrospun nanofibrous structure: a novel scaffold for tissue engineering, J. Biomed. Mater. Res. A 60 (4) (2002) 613–621.
[43] F. Nudelman, K. Pieterse, A. George, P.H. Bomans, H. Friedrich, L.J. Brylka, P.A. Hilbers, G. de With, N.A. Sommerdijk, The role of collagen in bone apatite formation in the presence of hydroxyapatite nucleation inhibitors, Nat. Mater. 9 (12) (2010) 1004.
[44] B. Harland, S. Walcott, S.X. Sun, Adhesion dynamics and durotaxis in migrating cells, Phys. Biol. 8 (1) (2011) 015011.
[45] M. Uddin, C. Hall, P. Murphy, Surface treatments for controlling corrosion rate of biodegradable Mg and Mg-based alloy implants, Sci. Technol. Adv. Mater. 16 (5) (2015) 053501.
[46] G.-y. Yuan, X.-b. Zhang, J.-l. Niu, H.-r. Tao, D.-y. Chen, Y.-h. He, Y. Jiang, W.-j. Ding, Research progress of new type of degradable biomedical magnesium alloys JDBM, Chin J Nonferrous Met 21 (2011) 2476–2488.
[47] F. Witte, J. Fischer, J. Nellesen, H.-A. Crostack, V. Kaese, A. Pisch, F. Beckmann, H. Windhagen, In vitro and in vivo corrosion measurements of magnesium alloys, Biomaterials 27 (7) (2006) 1013–1018.
[48] J. Zeng, L. Ren, Y. Yuan, Y. Wang, J. Zhao, R. Zeng, K. Yang, X. Mei, Short-term effect of magnesium implantation on the osteomyelitis modeled animals induced by Staphylococcus aureus, J. Mater. Sci. Mater. Med. 24 (10) (2013) 2405–2416.
[49] T.Y. Nguyen, C.G. Liew, H. Liu, An in vitro mechanism study on the proliferation and pluripotency of human embryonic stems cells in response to magnesium degradation, PLoS One 8 (10) (2013) e76547.
[50] Y.-D. Kwon, D.-W. Lee, S.-O. Hong, Magnesium vs. machined surfaced titanium-osteoblast and osteoclast differentiation, J Adv Prosthodont 6 (3) (2014) 157–164.
[51] R.A. Kaya, H. Çavuşoğlu, C. Tanik, A.A. Kaya, Ö. Duygulu, Z. Mutlu, E. Zengin, Y. Aydin, The effects of magnesium particles in posterolateral spinal fusion: an experimental in vivo study in a sheep model, J. Neurosurg. Spine 6 (2) (2007) 141–149.
[52] Y.G. Kang, J. Wei, J.W. Shin, Y.R. Wu, J. Su, Y.S. Park, J.-W. Shin, Enhanced biocompatibility and osteogenic potential of mesoporous magnesium silicate/polycaprolactone/wheat protein composite scaffolds, Int. J. Nanomed. 13 (2018) 1107.
[53] D. He, W. Dong, S. Tang, J. Wei, Z. Liu, X. Gu, M. Li, H. Guo, Y. Niu, Tissue engineering scaffolds of mesoporous magnesium silicate and poly (ε-caprolactone)–poly (ethylene glycol)–poly (ε-caprolactone) composite, J. Mater. Sci. Mater. Med. 25 (6) (2014) 1415–1424.
[54] C. Wu, Z. Chen, Q. Wu, D. Yi, T. Friis, X. Zheng, J. Chang, X. Jiang, Y. Xiao, Clinoenstatite coatings have high bonding strength, bioactive ion release, and osteoimmunomodulatory effects that enhance in vivo osseointegration, Biomaterials 71 (2015) 35–47.
[55] S. Castiglioni, V. Romeo, L. Locatelli, A. Cazzaniga, J.A.M. Maier, TRPM7 and MagT1 in the osteogenic differentiation of human mesenchymal stem cells in vitro, Sci. Rep. 8 (1) (2018) 16195.
[56] S.J. Morrison, D.T. Scadden, The bone marrow niche for haematopoietic stem cells, Nature 505 (7483) (2014) 327.
[57] B. Sacchetti, A. Funari, S. Michienzi, S. Di Cesare, S. Piersanti, I. Saggio, E. Tagliafico, S. Ferrari, P.G. Robey, M. Riminucci, Self-renewing osteoprogenitors in bone marrow sinusoids can organize a hematopoietic microenvironment, Cell 131 (2) (2007) 324–336.